J. Phys.: Condens. Matter **20** (2008) 335101 (9pp) doi:10.1088/0953-8984/20/33/335101

Influence of weak anchoring upon the alignment of smectic A liquid crystals with surface pretilt

R De Vita[1] **and I W Stewart**[2]

[1] Department of Engineering Science and Mechanics, Virginia Tech, 230 Norris Hall, Blacksburg, VA 24061, USA
[2] Department of Mathematics, University of Strathclyde, Livingstone Tower, 26 Richmond Street, Glasgow G1 1XH, UK

E-mail: devita@vt.edu and i.w.stewart@strath.ac.uk

Received 18 April 2008, in final form 4 June 2008
Published 8 July 2008
Online at stacks.iop.org/JPhysCM/20/335101

Abstract
Equilibrium configurations for smectic A liquid crystals in a 'bookshelf' geometry are determined from a nonlinear continuum model under strong and weak anchoring conditions at the boundary for the usual director **n**. Natural boundary conditions are derived for **n** and the smectic layer normal **a** when a preferred director orientation $\mathbf{n}_p$, which generally induces a director pretilt, is prescribed on the boundaries. Two key aspects are examined via the nonlinear equilibrium equations: the separation of **n** from **a** and the influence of weak anchoring. The orientations of **n** and **a** relative to $\mathbf{n}_p$ may differ significantly and depend very much upon the magnitude of the anchoring strength. These results from a nonlinear theory are natural and novel developments of previous classical linearized models for which $\mathbf{n} \equiv \mathbf{a}$. Comparisons are also drawn between solutions for strong and weak anchoring conditions.

1. Introduction

Liquid crystals are anisotropic fluids that consist of rod-like molecules which have a preferred local average orientation. This average orientation is described by the unit vector **n**, commonly called the director. The molecular alignment in smectic liquid crystals leads to a layered structure in which **n** is parallel to the local layer normal **a**. This is what is known as the smectic A (SmA) phase of liquid crystals and is shown schematically in figure 1(a) where the short bold lines represent the average molecular arrangement. However, it is known that **n** and **a** may separate close to the idealized SmA phase, leading to a local structure that is called the smectic C (SmC) liquid crystal phase where the angle between the director and the layer normal, denoted by ϑ, is non-zero and the director is locally constrained to lie on the surface of a fictitious cone having an axis parallel to **a**, as shown in figure 1(b). The angle ϑ, also called the smectic cone angle, is usually temperature dependent but it may also vary due to competition between preferred bulk and surface alignments and smectic layer compressional effects, as will be discussed in this paper. The idealized SmA liquid crystal phase is said to occur when $\vartheta \equiv 0$, in which case **n** and **a** coincide as in figure 1(a). In this paper we shall be concerned principally with liquid crystals that have an inherent desire to adopt the idealized SmA phase and we shall concentrate on how different boundary conditions can influence the orientation of the local layer structure and director alignment, especially as **n** and **a** separate close to the boundaries of a given sample.

When the SmC phase is present it is often necessary to introduce the unit orthogonal projection of **n** onto the local smectic planes, denoted by **c**, so that the local orientation of the director is given by $\mathbf{n} = \cos\vartheta\mathbf{a} + \sin\vartheta\mathbf{c}$, as shown in figure 1(a). The orientation angle ϕ of **c**, measured with respect to some fixed axis within the local smectic plane, is usually introduced and a complete description of the orientation **n** in SmC can then be given via the two orientation angles ϑ and ϕ because knowledge about the orientation of **a** and **c** is then equivalent to that for the orientation of **n**. Nevertheless, in a straightforward geometrical set-up, such as that to be introduced here, the orientation angle ϕ can be considered as fixed so that we can effectively set $\phi \equiv 0$. This is an assumption that is thought to be a good approximation in the description of planar aligned smectic liquid crystals when they are close to the SmA phase, especially when flow is neglected [1, 2]. For more general details on the physics and

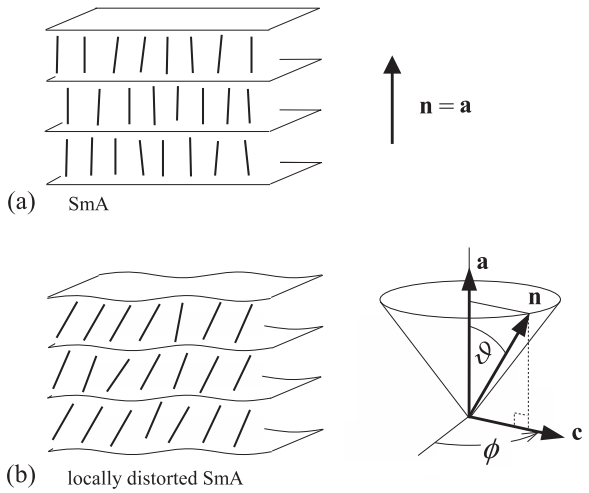

Figure 1. (a) An idealized planar layered SmA liquid crystal. The rod-like molecules are arranged in equidistant parallel layers as shown. The director **n**, represented by the short bold lines, and layer normal **a** coincide everywhere. (b) Fluctuation in the alignment of **n** and **a** occur due to competing boundary conditions or perturbations. Locally, **n** and **a** may separate by an angle ϑ to form a SmC phase where the director may align along the surface of a fictitious cone. The unit orthogonal projection of **n** onto the local smectic plane is denoted by **c** which allows an orientation angle ϕ to be defined relative to some fixed axis within the smectic planes. Both **a** and **n** may vary in space.

mathematical descriptions of SmA and SmC liquid crystals the reader is referred to the books by de Gennes and Prost [2] and Stewart [3].

The local planar layer structure of smectic liquid crystals may be described by a scalar function Φ, whereby the layer normal is always given by $\mathbf{a} = \nabla\Phi/|\nabla\Phi|$. For example, if uniformly aligned planar smectic layers, such as those depicted in figure 1(a), lie parallel to the xy plane then $\Phi = z$ leads to $\mathbf{a} = (0, 0, 1)$ in the usual Cartesian description. It is often convenient to employ both **a** and Φ when formulating mathematical descriptions. In equilibrium configurations it is known that the Oseen condition [4], $\nabla \times \mathbf{a} = \mathbf{0}$, holds when the smectic layers exhibit no dislocations. It has been common practice to assume that **n** and **a** always coincide when modelling fluctuations or changes to the alignment of SmA samples [2, 3]. However, there has been a resurgence of interest in the continuum modelling of SmA liquid crystals when, in a departure from the classical continuum description, **n** and **a** may separate [5–10] so that they, or equivalently, **n** and Φ, can provide a more realistic description of the director alignment. This also requires, in general, a relaxation of the Oseen condition when considering general disturbances or imposed realignments to the director and smectic layers. The Oseen condition will not be imposed here, although it should be noted that the theory below does not exclude the possibility that in special cases $\nabla \times \mathbf{a}$ may vanish over some region. The director orientation on the boundary of many samples can be considered as being fixed in a preferred orientation that is physically determined by an alignment technique, such as that discussed in [1]; such a fixed boundary condition is called strong anchoring and the director will always align on the boundary at the preferred surface alignment no matter what alignment may be induced in the bulk of the sample. More realistic boundary conditions can be modelled by what is known as weak anchoring. In this case the director alignment on the boundary is allowed to vary because of a competition between the director alignment in the bulk and the preferred surface alignment on the boundary; the director is thus weakly anchored to the boundary and the flexibility of the director alignment at the surface is controlled by a finite anchoring strength that is linked to a surface energy term. As the magnitude of the anchoring strength increases to infinity we recover the strong anchoring boundary conditions and for this reason strong anchoring is also called infinite anchoring. We shall look at strong and weak anchoring formulations and suppose in all cases that the director has a preferred alignment angle on the boundaries, to be introduced below. In all anchoring situations, **n** and **a** may vary significantly relative to each other, especially near the sample boundaries. A preferred surface alignment for the director will always be supposed while no imposed boundary conditions will be made upon the smectic layer orientation at the boundaries. The layer alignment at the boundaries will be calculated via the usual natural boundary conditions that arise in the classical calculus of variations so that the layers will adopt an alignment at the boundaries that follows naturally from any imposed preferred surface director alignment. This supplements the work of Stewart [10] where strong anchoring of the director and a supposed fixed smectic layer alignment at the boundaries were assumed in some preliminary studies of equilibrium configurations of SmA. The two key features of this present paper are, firstly, the consideration of equilibrium solutions for the director and smectic layers when **n** no longer necessarily coincides with **a** and, secondly, a comparison between the results for strong and weak anchoring of the director. In all cases, natural boundary conditions are imposed upon the smectic layer alignment.

We consider a sample of 'bookshelf' aligned SmA liquid crystal confined between boundary plates as shown in figure 2 below. The mathematical model, governing equilibrium equations and boundary conditions are discussed in section 2, together with elementary models for the bulk and surface energy densities. The special case of strong anchoring of the director with natural boundary conditions for the smectic layer tilt is discussed in section 3 while solutions for weak anchoring are investigated in section 4. A discussion of the results is given in section 5.

2. Model and equilibrium equations

Equilibrium configurations for bounded samples of SmA will be considered and the equilibrium equations for **n** and **a** will be obtained by minimizing the associated energy consisting of bulk and surface contributions. A bulk energy density, w, will be employed that is based upon the work of Auernhammer *et al* [5, 6, 11], Weinan [12], Ribotta and Durand [7], Soddemann *et al* [8] and Stewart [9]. It has the general form, when **n** is close to **a**,

$$w = \tfrac{1}{2}K_1^n(\nabla\cdot\mathbf{n})^2 + \tfrac{1}{2}K_1^a(\nabla\cdot\mathbf{a})^2 + \tfrac{1}{2}B_0\,(|\nabla\Phi| + \mathbf{n}\cdot\mathbf{a} - 2\,)^2 + \tfrac{1}{2}B_1\{1 - (\mathbf{n}\cdot\mathbf{a})^2\}, \tag{2.1}$$

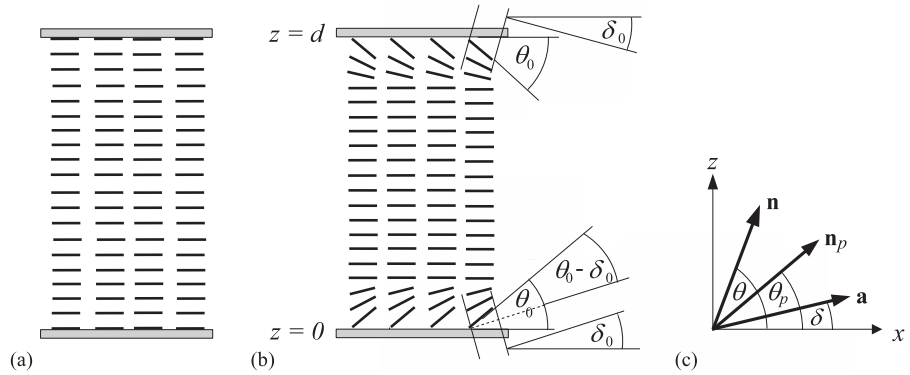

Figure 2. (a) The idealized bookshelf SmA alignment when the director **n**, represented by the short bold lines, coincides with the layer normal **a** and $\theta_0 = \theta_p = \delta_0 = 0$. The sample is confined between boundary plates located at $z = 0$ and d. (b) The boundary conditions for the director and layer normal are dictated by a competition between elastic effects in the bulk and the preferred director alignment θ_p at the boundary. For weak anchoring, the value of θ on the boundary, denoted by θ_0, will generally differ from θ_p. The smectic layer tilt at the boundary is δ_0 and is determined from classical natural boundary conditions. (c) Definitions of the orientation angles θ and δ for the director **n** and smectic layer normal **a**. The preferred director orientation on the boundary, $\mathbf{n}_p$, makes an angle θ_p, determined by physical alignment processes.

with the total bulk energy being given by the integral of w over the sample volume. The energy density w in (2.1) is invariant under the simultaneous changes in sign $\mathbf{n} \to -\mathbf{n}$ and $\mathbf{a} \to -\mathbf{a}$, which is equivalent to invariance under the simultaneous changes $\mathbf{n} \to -\mathbf{n}$ and $\nabla\Phi \to -\nabla\Phi$. The first term on the right-hand side of (2.1) represents the elastic splay deformation of the director **n** while the second term describes the bending of the smectic layers; both K_1^n and K_1^a are positive elastic constants. The third term is related to smectic layer compression and is an extended version of that which is known from the classical descriptions of SmA, based upon the results in [2, 6, 12]; B_0 is the positive layer compression constant. The fourth term accounts for the coupling between **n** and **a** with the positive constant B_1 having dimensions of energy per unit volume: in an equilibrium state this energy contribution is minimized when **n** and **a** are parallel. This term can also be written as $\frac{1}{2}B_1(\mathbf{n}\times\mathbf{a})^2$ because **n** and **a** are unit vectors, as used in [5, 6, 8]. The above model does not exclude the possibility that **n** and **a** may coincide at particular locations or regions.

In the conventional description of SmA the free energy density consists of layer compression and splay elasticity because the classical twist elasticity is necessarily absent while the bend elasticity contribution is considered as negligible. This approach has, in the first instance, led to the elementary energy density contributions appearing in (2.1) where the terms related to the bend elasticity of **n** and **a** have been neglected. Ribotta and Durand [7] have neglected bend in their model because the director and smectic layers are considered to be more sensitive to spatial variations in directions parallel to the smectic layers rather than along the smectic layer normal direction. A justification for omitting the bend term when $\mathbf{a} = \mathbf{n}$ has also been outlined by Weinan [12]. However, it should be mentioned that the omission of bend is not generally justified, especially near screw dislocations, as has been mentioned by Pleiner [13], who has noted that for large gradients the bend term can become comparable to the other gradient energy terms and can therefore no longer be considered negligible. Nevertheless, for the model introduced here we follow the initial procedures adopted by previous authors [5–8] and assume that bend will not be a dominant feature compared to splay, layer compression and the possible separation of **n** and **a**. A more detailed investigation involving the inclusion of bend is possible by suitably amending the energy density and following the numerical procedures that have been used below.

A weak anchoring surface energy density can be introduced in the form of Rapini–Papoular [3, 14]

$$w_s = \tfrac{1}{2}\tau_0\omega(\mathbf{n}\times\mathbf{n}_p)^2 = \tfrac{1}{2}\tau_0\omega\{1-(\mathbf{n}\cdot\mathbf{n}_p)^2\}, \tag{2.2}$$

where τ_0 has dimensions of surface tension (J m^{-2}), $\omega > 0$ is a dimensionless measure of the weak anchoring strength and $\mathbf{n}_p$ is the preferred director alignment at the boundary surface, usually prescribed by mechanical or surface treatment procedures. The total surface energy is the integral of w_s over the surface of the sample. In this formulation, the surface energy is minimized when **n** is parallel to $\mathbf{n}_p$. The total energy per unit volume is

$$W = \int_\Omega w\,\mathrm{d}\Omega + \int_S w_s\,\mathrm{d}S, \tag{2.3}$$

where Ω is the sample volume and S is its surface.

We shall examine what is commonly called the 'bookshelf' alignment of SmA. In a perfectly aligned sample of bookshelf SmA the director is parallel to the smectic layer normal and the planar smectic layers themselves are arranged in a bookshelf formation perpendicular to parallel planar boundaries, as shown in figure 2(a). Such an idealized alignment is only possible when $\mathbf{n}_p = \mathbf{n} = \mathbf{a}$, which is generally not the case. It will be assumed that the director **n** and the smectic layer normal **a** are uniform in the x and y

directions so that their respective orientation angles θ and δ, measured with respect to the x-axis as shown in figure 2(c), are functions of z only, i.e. $\theta = \theta(z)$ and $\delta = \delta(z)$. Note that the boundary orientation angle θ_p of the preferred director alignment $\mathbf{n}_p$ is fixed at the boundary. The anticipated director and smectic layer alignment in a bookshelf-type geometry across a sample of depth d in the z-direction is shown schematically in figure 2(b). The director $\mathbf{n}$ and the layer representation Φ may then assume the forms [10]

$$\mathbf{n} = (\cos\theta(z), 0, \sin\theta(z)), \tag{2.4}$$

$$\Phi(x, z) = x + \int_{z_0}^{z} \tan\delta(t)\,\mathrm{d}t, \tag{2.5}$$

where z_0 is an arbitrary constant. It follows immediately that

$$\nabla\Phi = (1, 0, \tan\delta(z)), \qquad |\nabla\Phi| = \sec\delta(z) \tag{2.6}$$

$$\mathbf{a} = \frac{\nabla\Phi}{|\nabla\Phi|} = (\cos\delta(z), 0, \sin\delta(z)), \tag{2.7}$$

$$\mathbf{n}\cdot\mathbf{a} = \cos(\theta(z) - \delta(z)). \tag{2.8}$$

It will be supposed that θ and δ will only take values strictly lying between $-\pi/2$ and $\pi/2$. From the expected symmetry of the problem, we look for solutions of the form

$$\theta(z) = -\theta(d - z), \qquad 0 \leqslant z \leqslant d, \tag{2.9}$$

$$\delta(z) = -\delta(d - z), \qquad 0 \leqslant z \leqslant d, \tag{2.10}$$

$$\theta'(0) = \theta'(d), \qquad \delta'(0) = \delta'(d), \tag{2.11}$$

where a prime denotes the differentiation with respect to z. The boundary conditions will then lead to

$$\begin{aligned} \theta(0) &= \theta_0, & \delta(0) &= \delta_0, \\ \theta(d) &= -\theta_0, & \delta(d) &= -\delta_0, \end{aligned} \tag{2.12}$$

for constant angles θ_0 and δ_0 that have to be determined from the minimization of the total energy when a given preferred orientation $\mathbf{n}_p$ for the director at the boundary is prescribed (see figure 2). These constant angles at the boundaries will be determined as part of the solution process and, despite being influenced by all the material parameters, they will be governed primarily by the magnitude of the weak anchoring strength $\tau_0\omega$ and the preferred director orientation angle θ_p at the boundaries. In general, $\theta_0 \neq \theta_p$ for weak anchoring whereas $\theta_0 = \theta_p$ under any strong anchoring assumptions.

The bulk energy density (2.1) becomes

$$\begin{aligned} w = {} & \tfrac{1}{2}K_1^n(\theta')^2\cos^2\theta + \tfrac{1}{2}K_1^a(\delta')^2\cos^2\delta \\ & + \tfrac{1}{2}B_0[\sec\delta + \cos(\theta - \delta) - 2]^2 + \tfrac{1}{2}B_1\sin^2(\theta - \delta). \end{aligned} \tag{2.13}$$

The preferred director orientation at the boundaries may be written as

$$\mathbf{n}_p^- = (\cos\theta_p, 0, \sin\theta_p), \qquad \mathbf{n}_p^+ = (\cos\theta_p, 0, -\sin\theta_p), \tag{2.14}$$

where θ_p is a fixed angle measured relative to the x-axis. The minus index refers to the preferred alignment angle of the director at the lower boundary $z = 0$ while the plus index refers to the preferred orientation at $z = d$. We remark that these preferred alignments, under weak anchoring, will never generally be achieved by the director because of competition with the minimization of the bulk energy. On the boundaries, given the conditions imposed upon θ in equation (2.12) and the forms for $\mathbf{n}_p^{\pm}$,

$$\begin{aligned} (\mathbf{n}\times\mathbf{n}_p^-)^2 &= \sin^2(\theta(0) - \theta_p), \\ (\mathbf{n}\times\mathbf{n}_p^+)^2 &= \sin^2(\theta(d) + \theta_p). \end{aligned} \tag{2.15}$$

Thus, from (2.12) and (2.15), the surface energy density on each boundary is given by

$$w_s = \tfrac{1}{2}\tau_0\omega\sin^2(\theta_0 - \theta_p), \tag{2.16}$$

since it easily seen that

$$w_s(\theta(0), \theta_p) = w_s(\theta(d), -\theta_p), \tag{2.17}$$

and this means that the total surface energy per unit area in the xy-plane on the boundaries (i.e. the surface integral appearing in (2.3)) for the problem described here is simply $2w_s$.

We shall minimize the functional W over a sample of depth d in the z-direction and of unit cross-sectional area in the xy-plane. We have

$$\begin{aligned} W = {} & \int_\Omega w\,\mathrm{d}\Omega + \int_S w_s\,\mathrm{d}S \\ = {} & \tfrac{1}{2}\int_0^d \{K_1^n(\theta')^2\cos^2\theta + K_1^a(\delta')^2\cos^2\delta \\ & + B_0[\sec\delta + \cos(\theta - \delta) - 2]^2 \\ & + B_1\sin^2(\theta - \delta)\}\,\mathrm{d}z + \tau_0\omega\sin^2(\theta_0 - \theta_p), \end{aligned} \tag{2.18}$$

subject to the aforementioned conditions in equations (2.9)–(2.12). Recall that θ_p is prescribed while θ_0 and δ_0 are to be determined. The coupled equilibrium equations for $\theta(z)$ and $\delta(z)$ in the bulk are identical to those previously obtained in [10] via the usual Euler–Lagrange equations, namely,

$$\begin{aligned} & K_1^n[\theta''\cos^2\theta - (\theta')^2\sin\theta\cos\theta] \\ & \quad + B_0[\sec\delta + \cos(\theta - \delta) - 2]\sin(\theta - \delta) \\ & \quad - B_1\sin(\theta - \delta)\cos(\theta - \delta) = 0, \end{aligned} \tag{2.19}$$

$$\begin{aligned} & K_1^a[\delta''\cos^2\delta - (\delta')^2\sin\delta\cos\delta] \\ & \quad - B_0[\sec\delta + \cos(\theta - \delta) - 2] \\ & \quad \times [\sec\delta\tan\delta + \sin(\theta - \delta)] \\ & \quad + B_1\sin(\theta - \delta)\cos(\theta - \delta) = 0, \end{aligned} \tag{2.20}$$

with θ and δ satisfying the boundary requirements in equation (2.12). The additional boundary conditions for weak anchoring of the director are well known in such circumstances (see, for example, [3, p 55] or [15] in the context of liquid crystals, or [16] in general) and are given by

$$\frac{\partial w}{\partial\theta_{,j}}\nu_j + \frac{\partial w_s}{\partial\theta} = 0, \tag{2.21}$$

$$\frac{\partial w}{\partial\delta_{,j}}\nu_j + \frac{\partial w_s}{\partial\delta} = 0, \tag{2.22}$$

where $\boldsymbol{\nu}$ is the outward normal to the boundary surfaces: in this present situation $\boldsymbol{\nu} = (0, 0, -1)$ at $z = 0$ and $\boldsymbol{\nu} = (0, 0, 1)$ at $z = d$. Inserting the form given explicitly in equation (2.15) into (2.13) and (2.16) leads to the additional requirements

$$\begin{gathered} 2K_1^n\theta'(0)\cos^2\theta_0 + \tau_0\omega\sin[2(\theta_\mathrm{p} - \theta_0)] = 0, \\ \delta'(0) = 0, \end{gathered} \tag{2.23}$$

at $z = 0$, given that in general we expect $\delta \neq \pm\pi/2$ (otherwise we would have the smectic layers parallel to the boundaries at the boundary surfaces). From the definition of $\mathbf{n}_\mathrm{p}^{\pm}$ in equation (2.14), coupled with taking the appropriate derivatives in θ in equation (2.15) and then applying the boundary conditions $\theta'(0) = \theta'(d)$ and $\theta(0) = -\theta(d)$, similar calculations reveal that the additional boundary conditions (2.23) must also hold at $z = d$.

2.1. The equations to be solved

It is expected that the director and the layer normal will accommodate themselves, via competition between preferred surface and bulk alignments, to be at the constant angles θ_0 and δ_0, respectively, on the boundaries and the determination of these angles is part of the problem to be solved. If we impose the aforementioned symmetry upon the solution then we may solve the system over the region $0 \leqslant z \leqslant d/2$ and obtain the solution for $d/2 \leqslant z \leqslant d$ via symmetry. The appropriate boundary conditions for our problem are then

$$\begin{gathered} 2K_1^n\theta'(0)\cos^2\theta_0 + \tau_0\omega\sin[2(\theta_\mathrm{p} - \theta_0)] = 0, \\ \theta(d/2) = 0, \qquad \delta(d/2) = 0, \qquad \delta'(0) = 0. \end{gathered} \tag{2.24}$$

Thus, in summary, we need to solve the equilibrium equations (2.19) and (2.20) subject to the boundary conditions stated in equations (2.24) for prescribed values of the preferred surface director alignment angle θ_p and the remaining material parameters K_1^n, K_1^a, B_0, B_1 and $\tau_0\omega$.

The equations (2.19), (2.20) and (2.24) can be non-dimensionalized by introducing the typical length scale λ ([2, p 344]), the dimensionless coupling constants B and κ, dimensionless anchoring strength τ and variable $\bar{z}$ by setting

$$\begin{gathered} \lambda = \sqrt{\frac{K_1^n}{B_0}}, \qquad B = \frac{B_1}{B_0}, \qquad \kappa = \frac{K_1^a}{K_1^n} \\ \tau = \frac{\lambda\tau_0\omega}{K_1^n}, \qquad \bar{z} = \frac{z}{\lambda}, \qquad \bar{d} = \frac{d}{\lambda}. \end{gathered} \tag{2.25}$$

The constants B and κ represent dimensionless measures of the anisotropy in the coupling and elastic constants, respectively. It is known that λ is often of the dimensions of the smectic interlayer distance [2]. Doing so reveals that they can be written as

$$\begin{aligned} &\theta''\cos^2\theta - (\theta')^2\sin\theta\cos\theta + [\sec\delta + \cos(\theta - \delta) - 2] \\ &\quad\times \sin(\theta - \delta) - B\sin(\theta - \delta)\cos(\theta - \delta) = 0, \end{aligned} \tag{2.26}$$

$$\begin{aligned} &\kappa\left[\delta''\cos^2\delta - (\delta')^2\sin\delta\cos\delta\right] - [\sec\delta + \cos(\theta - \delta) - 2] \\ &\quad\times [\sec\delta\tan\delta + \sin(\theta - \delta)] \\ &\quad + B\sin(\theta - \delta)\cos(\theta - \delta) = 0, \end{aligned} \tag{2.27}$$

where a prime now denotes differentiation with respect to $\bar{z}$. The relevant boundary conditions become

$$\begin{gathered} 2\theta'(0)\cos^2\theta_0 + \tau\sin[2(\theta_\mathrm{p} - \theta_0)] = 0, \qquad \theta(\bar{d}/2) = 0, \\ \delta(\bar{d}/2) = 0, \qquad \delta'(0) = 0. \end{gathered} \tag{2.28}$$

The weak anchoring problem has now been reduced to finding the solutions $\theta(\bar{z})$ and $\delta(\bar{z})$ to equations (2.26) and (2.27) with the boundary requirements (2.28).

It is expected [7] that B_1 should be comparable (perhaps smaller) to the more familiar compression constant B_0. We shall also suppose that K_1^a is similar in magnitude to K_1^n. Typical approximate values for the material parameters in liquid crystals may be taken as [3, 17]

$$K_1^n = 10^{-11}\ \mathrm{N}, \qquad \tau_0\omega = 10^{-5}\ \mathrm{J\ m^{-2}}. \tag{2.29}$$

The length scale λ is often around 20 Å [2], which leads to an estimate of $B_0 \sim 2.5 \times 10^6\ \mathrm{N\ m^{-2}}$. For a thin sample of depth $d = 2\ \mu\mathrm{m}$ we are led to consider $\bar{d} = 1000$ (it is common in experiments for d to be around $2 \sim 10\ \mu\mathrm{m}$, for example $d = 3.5\ \mu\mathrm{m}$ in the experiment by Elston [1]). Further, with the estimates in (2.29), we also arrive at the approximation $\tau \sim 10^{-3}$ as a possible typical estimate for the dimensionless anchoring strength. A typical value for θ_p that may be selected is around $\pi/6$, as has been reported from experiments [1]. We therefore choose, motivated by the results in [10], to base our work around the dimensionless parameters

$$\begin{gathered} B = 1, \qquad \kappa = 1, \qquad \bar{d} = 1000, \qquad \tau = 10^{-3}, \\ \theta_\mathrm{p} = \frac{\pi}{6}. \end{gathered} \tag{2.30}$$

Nevertheless, we shall also look at the influence upon various properties of the solutions as the parameters B, κ and τ vary in differing contexts.

2.2. A special case: the strong anchoring problem

In the strong anchoring case only the bulk energy is of interest because the anchoring strength τ becomes infinite and $\theta(0)$ is fixed at the preferred surface alignment angle θ_p. The equilibrium equations are again given by equations (2.26) and (2.27) while the boundary conditions for θ (again taken over the half-depth of the sample) are replaced by

$$\theta(0) \equiv \theta_0 = \theta_\mathrm{p}, \qquad \theta(\bar{d}/2) = 0. \tag{2.31}$$

From symmetry, $\delta(\bar{d}/2) = 0$, as before, but the boundary condition at $z = 0$ must be obtained by the usual natural boundary condition requirement [18, p 94], namely,

$$\left.\frac{\partial w}{\partial\delta'}\right|_{\bar{z}=0^+} = 0. \tag{2.32}$$

The boundary conditions for δ are therefore

$$\delta'(0) = 0, \qquad \delta(\bar{d}/2) = 0, \tag{2.33}$$

and are thus the same as in the weak anchoring case.

We shall begin by examining the strong anchoring case in order to draw comparisons with the weak anchoring results that will follow. We remark that when $\delta(0) = \delta_0$ is also prescribed or is known, that is, if strong anchoring of the layer alignment is given in addition to strong anchoring of the director, then the strong anchoring problem reduces to that discussed extensively by Stewart [10]. The strong anchoring problem solved in the next Section allows the solution for δ to select its natural boundary condition at $\bar{z} = 0$ so that the only boundary conditions that need to be supplied are those for θ, i.e. the value of θ_p.

3. Solutions for strong anchoring

For strong anchoring of the director, equations (2.26) and (2.27) with the boundary conditions (2.31) and (2.33) have been solved numerically for the dimensionless material parameters (2.30) (excluding τ, of course) using the dsolve routine in Maple 10 and the results can be seen in figure 3. The solutions for θ and δ have been plotted in figure 3(a) where it can be seen that they appear to be very close to each other over most of the sample and are both close to zero across the centre of the sample: this indicates that their alignment away from the boundaries is close to the idealized SmA bookshelf geometry when they are sufficiently far away from the boundaries. There is evidently a boundary layer in close proximity to each boundary where θ and δ differ greatly from zero as they adjust to satisfy their boundary conditions. Further, there is a significant separation between θ and δ in a region near each boundary. This separation shows that the smectic layers are bending in such a region and that the director is also considerably tilted relative to the layer normal. The inset in figure 3(a) shows the separation close to the boundary at $\bar{z} = 0$ while figure 3(b) shows the same solutions plotted, for emphasis, against a log scale over the domain $0.01 \leqslant \bar{z} \leqslant \bar{d}/2$. Similar to the situation reported in [10], it is apparent that there are really two boundary layer effects: the first boundary layer occurs as the director and layer normal reorient within a short distance from the boundary in an attempt to become mutually parallel (where $\theta \simeq \delta$): this demonstrates that the sample strives to adopt the idealized SmA phase as close to the boundary as possible. The second boundary layer effect occurs as the smectic layers themselves adjust as they in turn attempt to adopt a bookshelf SmA structure across the bulk of the sample. This phenomenon takes place over a much larger distance than that for which **n** and **a** initially reorient in their attempt to be coincident; both distances are, nevertheless, relatively small compared to the sample depth $\bar{d}$ and occur over length scales that are comparable to those reported in [10]. For example, when expressed in the original units, the first reorientation effect occurs over an approximate distance of 50–100 Å, which compares favourably with the experimental data reported by Chen *et al* [19] for a ferroelectric smectic liquid crystal. The smectic layer reorientation that happens in the second boundary layer occurs over a length of order 0.4 μm, and this is of the same order of magnitude as that observed experimentally by Elston [1] and Bonvent *et al* [20].

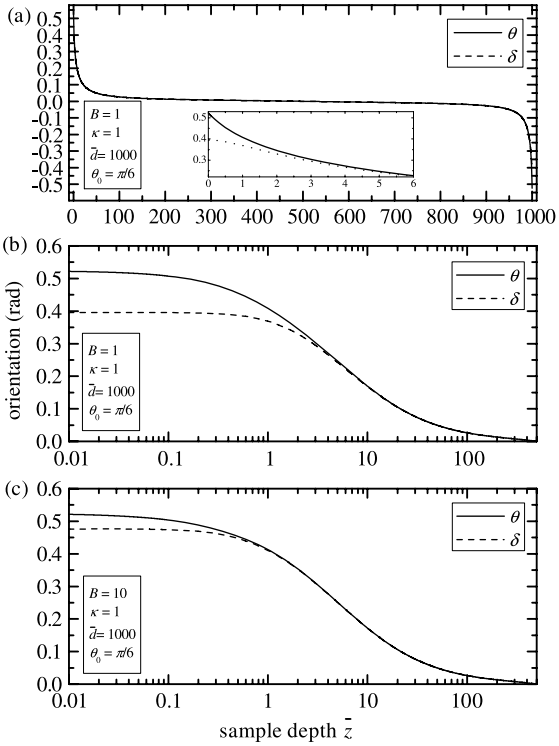

Figure 3. Solutions to equations (2.26) and (2.27) with the boundary conditions (2.31) and (2.33) for θ and δ plotted for strong anchoring of the director on the boundary at $\theta_0 \equiv \theta_p = \pi/6$ and the other parameters as indicated. (a) The full solutions on $[0, \bar{d}]$. These solutions appear to almost coincide over $[0, \bar{d}]$. The inset graph shows that the peak of the separation between θ and δ occurs near the boundary. (b) The solutions in (a) over a log scale on $[0.01, \bar{d}/2]$, highlighting the separation between θ and δ near the boundary at $\bar{z} = 0$. (c) The effect of increasing the coupling constant B from unity (in (b)) to 10.

A major point to note about the plots in figure 3 is that θ_0 has been fixed at θ_p while δ_0 on the boundary has to be determined and, unlike θ_0, will vary as the material parameters change. For example, if B is increased and the remaining constants are unaltered, which means that B_1 becomes larger, then δ_0 shifts closer to θ_0, as shown in figure 3(c) where $B = 10$ has been adopted. This is as expected because the magnitude of B_1 is a measure of the strength of the coupling between **n** and **a**: larger values of B should signify a reduction in the value of $|\delta(z) - \theta(z)|$. This difference when evaluated at the boundary provides a good indication of the impact that changing the parameters will have throughout the sample. The difference at the boundary is best expressed by considering the calculated values of the natural boundary condition δ_0 (determined from the full solution for $\delta(\bar{z})$) as key material parameters vary while θ_0 has been fixed, as is demonstrated by the plots presented in figure 4 where the material parameters, except for that which varies, are as indicated in the figure. For the typical material parameters shown in the figure, we allow only the dimensionless parameter $\kappa = K_1^a/K_1^n$ to vary in figure 4(a) in order to observe the dependence of δ_0 upon κ. As κ increases through unity, the elastic constant K_1^a becomes dominant and δ_0 decreases, which reflects the dominance of the bookshelf layer alignment. This shows

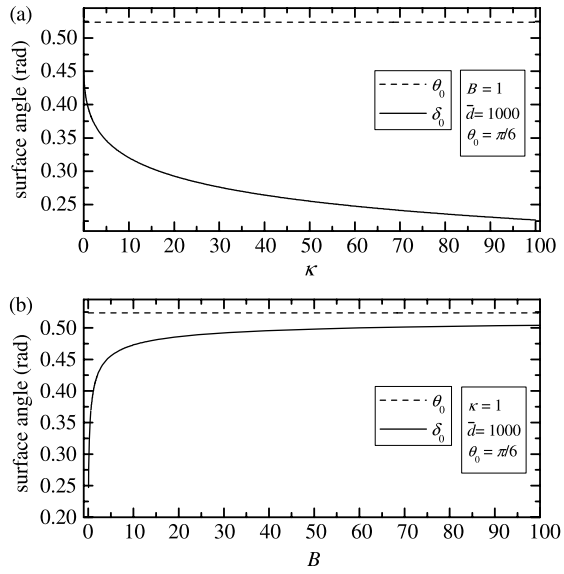

Figure 4. Solutions for the natural boundary condition δ_0 (obtained from the full solutions) plotted for the indicated parameters with strong anchoring of the director on the boundary set to $\theta_0 = \pi/6 \approx 0.524$. (a) The dependence of δ_0 upon the dimensionless parameter $\kappa = K_1^a/K_1^n$ with $B = 1$. (b) The dependence of δ_0 upon the dimensionless parameter $B = B_1/B_0$ with $\kappa = 1$.

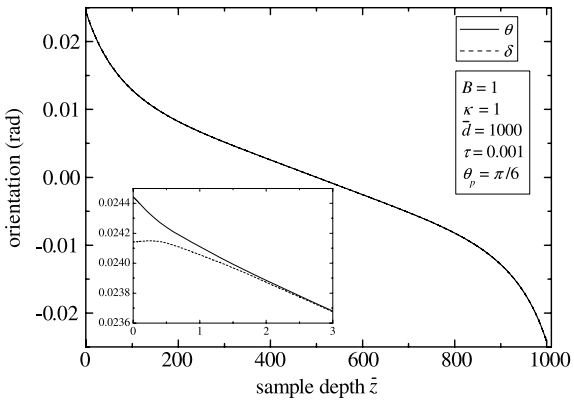

Figure 5. Solutions to equations (2.26) and (2.27) for θ and δ subject to the weak anchoring conditions in (2.28), plotted for the indicated parameters. The effects of weak anchoring are prominent near the boundary and are displayed in the inset.

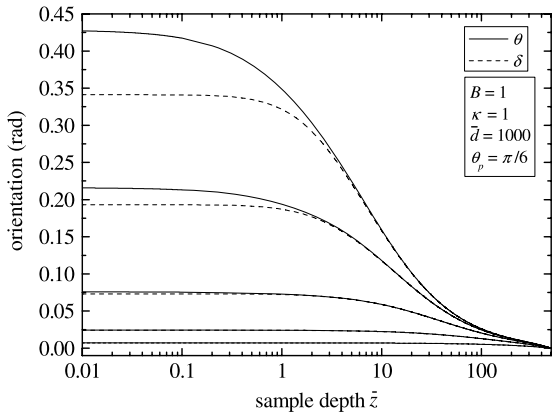

Figure 6. Solutions to equations (2.26) and (2.27) for θ and δ subject to the weak anchoring conditions in (2.28) plotted over the interval $[0.01, \bar{d}/2]$ on a log scale for the indicated parameters. The pairs of solutions for θ and δ correspond to the values of $\tau = 10^{-4}$, 10^{-3}, 10^{-2}, 10^{-1} and 1: as τ increases each pair of solutions correspondingly increase near the boundary, as shown.

that the bookshelf alignment becomes more prevalent near the boundary, and therefore across more of the central bulk of the sample, as K_1^a increases: this is as expected because this layer bending elastic constant will dominate the director splay constant K_1^n. In figure 4(b) only the parameter B varies. As anticipated from the result in figure 3(b), as B increases, that is, as B_1 increases relative to B_0, **n** and **a** attempt to be as parallel to each other as possible and therefore δ_0 strives to coincide with θ_0 at the boundary. Moreover, it is seen that as B decreases the layer structure near the boundary will tend towards the bookshelf structure since δ_0 is decreasing; further, as the coupling between **n** and **a** weakens and δ_0 decreases, the separation between θ_0 and δ_0 increases.

4. Solutions for weak anchoring

For weak anchoring of the director, equations (2.26) and (2.27) have been solved numerically subject to the boundary requirements (2.28). As an example, solutions have been found for the typical material parameters in (2.30) and the results are displayed in figure 5. The solutions for θ and δ virtually coincide over most of the sample depth: however, as shown in the inset in figure 5, there is a separation between these solutions near the boundary. The separation in this particular example is relatively small, but it does show that a boundary layer effect is again to be anticipated and therefore further solutions have been calculated for the same fixed material parameters with the exception of the anchoring strength τ, which we allow to vary in order to determine the influence of the anchoring strength. Figure 6 presents calculated solutions for the parameters indicated in the figure for the selected values of $\tau = 10^{-4}$, 10^{-3}, 10^{-2}, 10^{-1} and 1. As τ increases through these values, the corresponding pairs of solutions, plotted in figure 6 on a log scale over $[0.01, \bar{d}/2]$ for emphasis, evidently increase in magnitude near the boundary. The solutions for $\tau = 10^{-3}$ (which have $\theta_0 \simeq \delta_0 \sim 0.024$ in figure 6) correspond to the particular solutions shown in figure 5. It is clear from figure 6 that the separation of the solutions $\theta(\bar{z})$ and $\delta(\bar{z})$ increases as τ increases and that both θ_0 and δ_0 also increase accordingly. It is also readily seen from figures 5 and 6 that there are boundary layer effects which are analogous to those described in the previous Section for strong anchoring. One striking observation is that the length scales over which the boundary effects take place are similar for both strong and weak anchoring. For example, we can compare the results displayed in figure 3(b) (strong anchoring) and figure 5 (weak anchoring), which have the same set of dimensionless material parameters except for τ, which is finite in figure 5. The main apparent differences are the magnitudes of θ_0 and δ_0 and their relative separation at the boundary. Weak anchoring conditions can vastly reduce these values compared

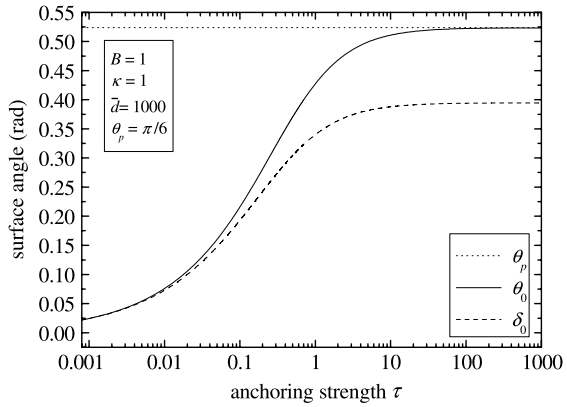

Figure 7. The dependence of the boundary surface angles θ_0 and δ_0 upon the anchoring strength τ for the indicated values of B, κ, $\bar{d}$ and θ_p.

to the preferred director alignment θ_p on the boundary. As the anchoring strength τ increases, it is seen in figure 6 that θ_0 is attracted towards its preferred boundary alignment of θ_p while δ_0 adjusts to its natural boundary condition.

The above solutions, obtained numerically via Maple, involved the determination of θ_0 and δ_0 as τ varied. Analogous to the results in figure 4 above, it is of importance to examine the boundary orientation angles and their dependence, not on B or κ, but on the weak anchoring parameter τ so that the influence of weak anchoring when other material parameters are fixed can be seen. This will also allow a comparison with the results for strong anchoring as τ increases. Figure 7 shows the dependency of the boundary angles θ_0 and δ_0 as τ varies. For very weak anchoring, these angles are both very close to each other and are relatively small compared to the preferred surface alignment angle θ_p. Such weak anchoring indicates that the preferred surface alignment has little effect upon the orientation of the director or the smectic layering and that the sample is close to achieving a uniform bookshelf SmA alignment because both **n** and **a** virtually coincide at the boundary and are almost parallel to the boundary surfaces. Nevertheless, the non-zero preferred surface alignment θ_p continues to influence the boundary angles, although its persistent effect is reduced by weak anchoring. It is further seen from figure 7 that as τ increases, θ_0 tends to its preferred boundary surface alignment θ_p while δ_0 tends to its natural boundary condition that can be determined under the assumption of strong anchoring. In this particular example, it is seen in figure 7, for the indicated material parameters, that δ_0 tends to the value identified under the strong anchoring assumption in figures 3(b), 4(a) (at $\kappa = 1$) and 4(b) (at $B = 1$) where $\delta_0 \approx 0.39$ rad. In other words, as the dimensionless anchoring strength τ increases it is clear from the numerical results that θ_0 and δ_0 tend to their corresponding values obtained in the strong anchoring case. Moreover, it is seen in figure 7 that the separation between θ_0 and δ_0 on the boundary increases as the anchoring strength increases.

5. Discussion

A mathematical model for the equilibrium profiles of SmA has been investigated for samples that are close to a 'bookshelf' geometry. The bulk equilibrium equations are given by (2.26) and (2.27) and are subject to the boundary conditions and requirements (2.31) and (2.33) in the case of strong (infinite) anchoring of the director at the boundary, and conditions (2.28) under weak (finite) anchoring.

Strong anchoring formulations were derived and discussed in section 3 and two boundary layer effects were identified in the corresponding solutions: the first boundary layer phenomenon occurred as the smectic layer normal and the director attempted to coincide in a region very close to the boundary; the second boundary layer effect showed a reorienting of the smectic layers themselves towards an idealized SmA bookshelf alignment. Such solutions were plotted numerically in figure 3. The surface pretilt θ_0 of the director was fixed while the natural boundary value δ_0 for the surface tilt of the smectic layers was calculated numerically; its dependence on the dimensionless parameters κ and B was displayed in figure 4. Comparisons with earlier theoretical results [10] for prescribed δ_0 were also made, in addition to comparisons with the experimental work contained in [1, 19, 20]. Strong anchoring in smectics with a variable director tilt relative to the smectic layer normal has also been discussed by McKay and Leslie [21] and McKay [22], who also discussed a geometrical set-up similar to that in figure 2(b) above. Despite some differences in the nonlinear smectic energy density used, the mathematical approach for strong anchoring employed in [21, 22] is similar in style to that presented here.

The influence of weak anchoring was determined in section 4 and solutions were obtained numerically to produce the results in figures 5–7. Although the boundary layer effects were similar to those discussed above for strong anchoring, there were great differences in the determination, and values, of θ_0 and δ_0 at the boundaries. The effects of weak anchoring were most prominent near the boundary where the magnitude of the anchoring strength τ controlled the magnitudes of θ_0 and δ_0 and their relative separation. The results in figure 7 are particularly revealing in that they show how these boundary values and their separation at the boundary depend upon τ. Additionally, figure 7 shows that as τ increases we recover the boundary conditions that were identified in figures 3(b) and 4 in the strong anchoring case.

As reviewed by Handschy and Clark [23], general surface and smectic layer tilt conditions in ferroelectric SmC liquid crystals (in which the smectic layers are close to a bookshelf alignment) can be quite complex and may possess significant coupling effects between the orientation angle ϕ, introduced in figure 1, and the smectic layer tilt at the boundary. Such coupling has been neglected here. However, the solutions described in sections 3 and 4 above exhibit SmC behaviour near the boundary and it may well be the case that a more intricate structure for the layer tilt at the boundaries is available, one that also varies along the x-direction (see especially figure 19 in [23]). This would also involve

director and layer orientations that would then have complex dependency on x and z while the complete structure would be uniform in the y-direction. Other more sophisticated boundary conditions (such as circular boundary conditions) can also be envisaged [23] and could be investigated in the cases of strong and weak anchoring. In many of these instances there will be a surface twist of the director in addition to the surface tilt that is described here. Recent work on weak anchoring for surface twist with no director tilt has been carried out on nematics by McKay *et al* [24], based on the work of Rapini–Papoular [14] and Belyakov *et al* [25], and these results will provide motivation for examining the problems discussed here in the context of more involved boundary phenomena. Although the aforementioned details are in the context of ferroelectric smectics, they are directly relevant to the understanding of the induced SmC phase discussed here for SmA samples. General discussions on weak director anchoring that incorporate the Rapini–Papoular form (2.2) as a special case can be found in Yokoyama and van Sprang [17] and Zhao *et al* [26]. Future work could also look at mixed boundary conditions that would destroy the symmetry assumptions made in the solutions presented above, for example, strong anchoring could be imposed on one boundary and weak anchoring at the other.

Distortions or perturbations to any of the SmA alignments discussed here may be possible via the application of an externally applied electric or magnetic field across the boundary plates. This would entail the addition of a magnetic or electric energy density to that stated in equation (2.1). In nematic liquid crystals it is known that if the director is pretilted under strong anchoring conditions then there is a constant equilibrium configuration ($\theta \equiv \theta_p$) that is available when no field is applied and that this alignment will always be distorted for any non-zero field magnitude, although it is not readily detectable until the field magnitude is sufficiently large (see [3, section 3.4.2] for details). A similar scenario in terms of the static solutions presented here will form the basis of future work, especially in relation to the stability of these structures and their responses to arbitrary small fluctuations: infinite samples of SmA are known to be dynamically stable to periodic time-dependent perturbations in both the classical case ($\mathbf{n} \equiv \mathbf{a}$ [12]) and for the model presented above (where $\mathbf{n} \not\equiv \mathbf{a}$ [9]) and a similar analysis remains to be tackled for the bookshelf and other confined geometries of SmA. In the context of electric field effects in confined lamellar systems the recent paper by Senyuk *et al* [27] has revealed some spectacular effects that have been investigated in three dimensions using the technique of fluorescence confocal polarizing microscopy (FCPM) [28]. Threshold and post-threshold phenomena such as layer undulations and buckling have been reported and the experimental observations just above a critical electric field magnitude near the boundary of a cell with weak anchoring in figure 8(b) in [27] will be of direct relevance to the work in this present paper once an electric energy density has been incorporated into the model. Layer undulations, layer tilting and buckling are the next natural phenomena to be investigated theoretically as extensions to the mathematical model presented here.

References

[1] Elston S J 1994 *Liq. Cryst.* **16** 151
[2] de Gennes P G and Prost J 1993 *The Physics of Liquid Crystals* 2nd edn (Oxford: Oxford University Press)
[3] Stewart I W 2004 *The Static and Dynamic Continuum Theory of Liquid Crystals* (London: Taylor and Francis)
[4] Oseen C W 1933 *Trans. Faraday Soc.* **29** 883
[5] Auernhammer G K, Brand H R and Pleiner H 2000 *Rheol. Acta* **39** 215
[6] Auernhammer G K, Brand H R and Pleiner H 2002 *Phys. Rev.* E **66** 061707
[7] Ribotta R and Durand G 1977 *J. Physique* **38** 179
[8] Soddemann T, Auernhammer G K, Guo H, Dünweg B and Kremer K 2004 *Eur. Phys. J.* E **13** 141
[9] Stewart I W 2007 *Contin. Mech. Thermodyn.* **18** 343
[10] Stewart I W 2007 *J. Phys. A: Math. Theor.* **40** 5297
[11] Auernhammer G K, Brand H R and Pleiner H 2005 *Phys. Rev.* E **71** 049901(E)
[12] Weinan E 1997 *Arch. Ration. Mech. Anal.* **137** 159
[13] Pleiner H 1988 *Liq. Cryst.* **3** 249
[14] Rapini A and Papoular M 1969 *J. Physique* **30** (C4) 54
[15] Jenkins J T and Barratt P J 1974 *Q. J. Mech. Appl. Math.* **27** 111
[16] Courant R and Hilbert D 1953 *Methods of Mathematical Physics* vol 1 (New York: Interscience)
[17] Yokoyama H and van Sprang H A 1985 *J. Appl. Phys.* **57** 4520
[18] Sagan H 1992 *Introduction to the Calculus of Variations* (New York: Dover)
[19] Chen W, Ouchi Y, Moses T and Shen Y R 1992 *Phys. Rev. Lett.* **68** 1547
[20] Bonvent J J, van Haaren J A M M, Cnossen G, Verhulst A G H and van der Sluis P 1995 *Liq. Cryst.* **18** 723
[21] McKay G and Leslie F M 1997 *Eur. J. Appl. Math.* **8** 273
[22] McKay G 2004 *J. Non-Newton. Fluid Mech.* **119** 115
[23] Handschy M A and Clark N A 1984 *Ferroelectrics* **59** 69
[24] McKay G, Kidney K J and Stewart I W 2007 *Mol. Cryst. Liq. Cryst.* **478** 57
[25] Belyakov V A, Osipov M A and Stewart I W 2006 *J. Phys.: Condens. Matter* **18** 4443
[26] Zhao W, Wu C and Iwamoto M 2002 *Phys. Rev.* E **65** 031709
[27] Senyuk B I, Smalyukh I I and Lavrentovich O D 2006 *Phys. Rev.* E **74** 011712
[28] Smalyukh I I, Shiyanovskii S V and Lavrentovich O D 2001 *Chem. Phys. Lett.* **336** 88